Ab Initio Study of the Ground and Excited States of Zinc Carbide, ZnC

Andromache Tsouloucha, Ioannis S. K. Kerkines, and Aristides Mavridis*

Laboratory of Physical Chemistry, Department of Chemistry, National and Kapodistrian University of Athens, P.O. Box 64 004, 157 10 Zografou, Athens, Greece

Received: March 10, 2003; In Final Form: May 20, 2003

The experimentally unknown molecule ZnC has been studied using multireference methods in conjunction with quantitative basis sets. Full potential energy curves have been constructed for the ground ($X\ ^3\Sigma^-$) state and 29 excited states, focusing mainly on dissociation energies and bonding mechanisms. The $X\ ^3\Sigma^-$ state of ZnC has a binding energy of 26.1 kcal/mol at the internally contracted multireference−(valence) configuration interaction level of theory (MRCI), whereas this value reduces to 23.3 kcal/mol upon including core−valence correlation effects ($3d^{10}$ of Zn) plus one-electron Douglas−Kroll relativistic corrections.

1. Introduction

In an ongoing effort to elucidate the electronic structure and bonding mechanisms of the first-row transition-metal diatomic carbides (neutrals and cations), we have recently studied the ground and low-lying excited states of ScC,[1] TiC,[2] FeC,[3] ScC^+,[4,5] TiC^+,[4,5] VC^+,[5,6] and CrC^+,[5,6] using highly correlated ab initio methods. We have extended this study to the diatomic carbides of Ca and Zn, the isovalent ($4s^2$) elements "bracketing" the first transition-metal element row. Very recently,[7,8] we have calculated the ground $X\ ^3\Sigma^-$ state and several excited states of the CaC molecule employing multireference configuration interaction (MRCI) methods. The present work will be focused on a similar investigation of ZnC.

While there is a complete absence of experimental results on the carbides BeC and MgC, and only a very recent electron-spin resonance experiment on CaC by Ziurys and co-workers,[9] theoretical work, albeit very limited, had definitely shown that the ground state of MgC is of $^3\Sigma^-$ symmetry, with the first excited state ($a\ ^5\Sigma^-$) 10.1 kcal/mol higher.[10] This is not the case, however, for CaC or BeC.[11] In particular, for CaC, only very recently and after some controversy,[12] theory showed[7,13] and experiment confirmed[9] that the $^3\Sigma^-$ is indeed the ground state. In all three carbides MC (M = Be, Mg, and Ca) the $^3\Sigma^-$ correlates to $M(ns^2;{}^1S) + C({}^3P)$, with a strongly competitive $^5\Sigma^-$ state correlating to $M(ns^1np^1;{}^3P) + C({}^3P)$. The interplay between the atomic energy separations $M({}^3P) \leftarrow M({}^1S)$ and the binding energies of the $^3\Sigma^-$ and $^5\Sigma^-$ states dictates ultimately the ground state of MC systems.

A similar $^3\Sigma^-$, $^5\Sigma^-$ antagonism could, in principle, exist in ZnC, but it would probably be hindered by the much larger $^3P \leftarrow {}^1S$ energy separation in Zn (4.054 eV) than, for instance, that in Ca (1.892 eV).[14] To the best of our knowledge, no experimental data have ever been published for ZnC. Boldyrev and Simons have performed a comparative theoretical study among the diatomics composed of Zn plus a first- or second-row main-group element.[15] At the quadratic configuration interaction, at the QCISD(T)/6-311++G(2d,2f) level of theory, and with the inclusion of the $3d^{10}$ electrons of Zn in their correlation treatment, they predict a ground $^3\Sigma^-$ state, with the $^5\Sigma^-$ state being 23.9 kcal/mol higher. At the same level of theory, the $^3P \leftarrow {}^1S$ energy separation in Zn is found to be equal to 3.82 eV.[15] The same authors have also performed calculations near the equilibrium for two other excited states of $^3\Pi$ symmetry. Quite recently, Kerkines et al.[8] tested the newly developed multireference Brillouin−Wigner coupled-cluster method (MRBWCCSD) against a variety of single and multireference methods for the $^5\Sigma^- \leftarrow {}^3\Sigma^-$ T_e gaps of both CaC and ZnC, employing large basis sets. All multireference methods converged to a T_e value for ZnC of at least 22−24 kcal/mol.[8]

2. Technical Details

As already mentioned, the first excited state of Zn is of ^3P symmetry with a $4s^14p^1$ configuration and an experimental $^3P \leftarrow {}^1S$ energy gap of 4.054 eV.[14] Corresponding values for the low-lying states of C are $({}^5S, {}^1S, {}^1D \leftarrow {}^3P) = (1.260, 2.084, 4.179$ eV), respectively.[14] Therefore, the lowest six ZnC dissociation channels in ascending energy order are $(Zn + C) = ({}^1S + {}^3P, {}^1S + {}^1D, {}^1S + {}^1S, {}^3P + {}^3P, {}^1S + {}^5S,$ and $^3P + {}^1D)$, the sixth one lying 5.314 eV above the $Zn({}^1S) + C({}^3P)$ ground-state atoms. Out of the 34 different $^{2S+1}|\Lambda|$ molecular states emerging from these six channels, 30 are examined in the present work.

The augmented triple-ζ atomic natural orbital (ANO) basis set of Roos and co-workers (21s15p10d6f4g)[16] was employed for Zn. For the C atom, the quadruple-ζ correlation-consistent basis set of Dunning and co-workers supplied with diffuse functions due to the expected negatively charged character of C in ZnC, aug-cc-pVQZ (13s7p4d3f2g), was chosen.[17] Generalized contraction of these sets to $[8s7p5d3f2g]_{Zn}/[6s5p4d3f2g]_C$ resulted in a one-electron basis set of 173 contracted spherical (5d, 7f, and 9g) Gaussian functions. Ground-state basis set superposition errors estimated with the Boys−Bernardi counterpoise scheme[18] do not exceed 0.1 kcal/mol at the equilibrium distance, and they were neglected thereafter.

Full potential energy curves (PECs) were calculated for 30 ZnC states at the internally contracted[19] level of theory. The complete active space (CASSCF) reference wave function was obtained by distributing the six valence electrons to the eight orbitals spanning the (4s + 4p) and (2s + 2p) valence orbital spaces of Zn and C, respectively. Technical difficulties in the calculation of the $^5\Sigma^-(2)$ and $^5\Sigma^-(3)$ states (vide infra) forced the addition of a ninth orbital in the active space for these two states only, correlating to the 5s orbital of Zn. Even though all our calculations were performed under C_{2v} symmetry

10.1021/jp030319g CCC: $25.00
Published on Web 07/12/2003

TABLE 1: Ground State Energies *E* (hartree) of the Zn (^{1}S) and C (^{3}P) Atoms, and Atomic Energy Separations ΔE (eV) at Different Levels of Theory

	Zn			C			
method	$-E$	$\Delta E(^3\text{P}\leftarrow{}^1\text{S})$	$\Delta E(^1\text{P}\leftarrow{}^1\text{S})$	$-E$	$\Delta E(^1\text{D}\leftarrow{}^3\text{P})$	$\Delta E(^1\text{S}\leftarrow{}^3\text{P})$	$\Delta E(^5\text{S}\leftarrow{}^3\text{P})$
NHF[a]	1777.848 12			37.688 619			
SCF	1777.847 28	2.592		37.688 323			
sa-SCF[b]	1777.847 28	2.644		37.688 256	1.558	3.782	2.437
CASSCF	1777.878 73[c]	3.499[c]	5.840[c]	37.705 611	1.573	2.602	2.909
MRCI	1777.881 29	3.423	5.404	37.785 224	1.275	2.675	4.114
MRCI+Q[d]				37.788 2	1.25	2.69	4.18
MRCI(d^{10})[e]	1778.329 33	3.777	5.859				
MRCI(d^{10})+Q[d,e]	1778.352 8	3.83	5.80				
MRCI(d^{10})/Rel[e,f]	1794.722 63	3.858					
MRCI+Q(d^{10})/Rel[d-f]	1794.748 4	3.95					
RCCSD	1777.881 29	3.412					
RCCSD(T)(d^{10})[e]	1778.368 12	3.846					
expt[g]		4.054	5.796		1.260	2.680	4.179

[a] Numerical Hartree−Fock, ref 26. [b] Spherically averaged SCF. [c] CASSCF with two electrons in four orbitals. [d] MRCI+multireference Davidson correction. [e] The $3d^{10}$ electrons of Zn were included in the correlation treatment. [f] Relativistic effects included via the Douglas−Kroll approximation. [g] Reference 14, M_J average.

restrictions, care was taken that all CASSCF wave functions display pure angular momentum symmetry (Λ) along the molecular axis.

With the exception of the X $^3\Sigma^-$, $^5\Sigma^-(1)$, and $^3\Pi(1)$ states, the state-average (SA) approach[20] was used throughout the CASSCF calculations. Energy losses for the X $^3\Sigma^-$ state at the MRCI level due to the SA approach are ~1.7 mE_h for the total energy and ~0.2 kcal/mol for the dissociation energy (D_e), leaving the predicted bond length (r_e) practically unaffected. Depending on symmetry and spin, the size of the CASSCF expansions ranges from 104 to 384 configuration functions (CFs). Respective values for the uncontracted and internally contracted MRCI expansions keeping 30 core electrons "frozen" are $\sim 3.3 \times 10^6$ and $\sim 1.0 \times 10^6$ CFs. Size-nonextensivity errors for this $6e^-$ treatment are of about 1 mE_h. For the sake of comparison, the ground X $^3\Sigma^-$ state was also studied using the restricted coupled cluster singles and doubles, with a perturbative triples estimate, RCCSD(T) method, and the multireference averaged coupled-pair functional, MRACPF method.[21] The effect of the Zn $3d^{10}$ "semicore" electrons on the calculated properties of ZnC was examined by allowing them to correlate in the MRCI treatment for all bound states around their equilibrium distances. In this case, the largest MRCI expansion contains $\sim 170 \times 10^6$ CFs, internally contracted to $\sim 6.8 \times 10^6$ CFs. Size-nonextensivity errors now increase, as expected, to an average value of 15 mE_h (~4 mE_h at the MRCI+Davidson correction = MRCI+Q level).

Relativistic effects were estimated for the X $^3\Sigma^-$ and $^5\Sigma^-(1)$ states following the one-electron Douglas−Kroll (DK) approximation,[22] employing the DK-recontracted aug-cc-pVQZ basis for C,[23] while leaving uncontracted the Roos ANO-TZ basis set of Zn.

For all 30 states we report total energies E, binding energies D_e, bond lengths r_e, harmonic and anharmonic vibrational frequencies ω_e and $\omega_e\chi_e$, rotation−vibration coupling parameters α_e, dipole moments μ, and Mulliken charges. Spectroscopic constants were extracted by solving the rovibrational nuclear Schrödinger equation using a Numerov technique.[24]

All calculations were performed with the MOLPRO 2002 suite of codes.[25]

3. Results and Discussion

Zn and C Atoms. Table 1 presents total energies for the ground Zn(^{1}S) and C(^{3}P) states, as well as atomic energy splittings among their low-lying valence excited states, at different levels of theory. The SCF energies for Zn(^{1}S) and C(^{3}P; spherically averaged) are less than 1 mE_h higher than the corresponding numerical Hartree−Fock values.[26] Although the MRCI energy splittings for C are in very good agreement with the experimental ones,[14] the rather crucial, for this work, $^3\text{P} \leftarrow {}^1\text{S}$ energy gap of Zn is predicted to be ~0.6 eV smaller than the experimental one at the MRCI(=CISD) level of theory. Upon correlation of the $3d^{10}$ electrons of Zn, this difference becomes less than half (~0.25 eV), indicating the necessity of their inclusion in the correlation treatment for one to obtain trustworthy T_e values for Zn. Inclusion of one-electron relativistic effects decreases even further the $^3\text{P} \leftarrow {}^1\text{S}$ difference to 0.20 eV, or 0.10 eV including the Davidson correction.

In what follows next, we will discuss separately the states emanating from each Zn + C dissociation channel. The first subsection, however, will be devoted explicitly to the ground X $^3\Sigma^-$ and first excited $^5\Sigma^-$ states (but see below). With the exception of the ground-state marked X, all other states will be denoted with a number in parentheses indicating the state ordering within a given symmetry manifold.

Table 2 lists our numerical findings for all 30 calculated states of ZnC, while Table 3 presents the adiabatic asymptotic channels $|\text{Zn}\rangle|\text{C}\rangle$, leading CASSCF configurations, and Mulliken atomic populations for each state. The molecular orbital (MO) numbering refers to the energy ordering within the valence (active) space. The MRCI potential energy curves for all states are depicted in Figure 1.

X $^3\Sigma^-$ and $^5\Sigma^-(1)$ States. As is evidenced from Table 3, the X $^3\Sigma^-$ state is dominated at equilibrium by two CFs. Although the second CF contributes only ~9% ($=|-0.31|^2$) to the equilibrium CASSCF wave function, its presence is crucial in obtaining reliable binding energies: indeed, an RCCSD(T) calculation using the "0.89" CF as reference gives $D_e = 18.3$ kcal/mol, ~8 kcal/mol lower than our MRCI value (Table 2). Kerkines et al.[8] have already demonstrated the inability of most single reference methods in obtaining accurate D_e and r_e values for CaC and ZnC. This can be attributed to the 4s4p near-degeneracy of the Zn atom, as the 3σ MO responsible for the multireference character of ZnC correlates asymptotically to the $4p_z$ atomic orbital of Zn. The same can also be seen by comparing the SCF and CASSCF $^3\text{P} \leftarrow {}^1\text{S}$ atomic splittings of Zn; the SCF splitting is much underestimated compared to the CASSCF one due to the poor (single reference) description of the ^{1}S ($4s^2$) state of Zn (Table 1).

TABLE 2: Total Energies E (hartree), Dissociation Energies D_e (kcal/mol), Bond Lengths r_e (Å), Harmonic and Anharmonic Frequencies ω_e and $\omega_e x_e$ (cm^{-1}), Rotation−Vibration Constants α_e (cm^{-1}), Dipole Moments μ (D), Mulliken Charges on Zn q_{Zn}, and Energy Gaps T_e (kcal/mol) of 30 States of the ZnC Molecule at the Internally Contracted MRCI/MRCI+Q Level of Theory[a]

state[b]	method	$-E$	D_e[c]	r_e	ω_e	$\omega_e x_e$	α_e ($\times 10^{-3}$)	μ[d]	q_{Zn}	T_e
$X\ ^3\Sigma^-$	CASSCF	1815.619 47	20.8	2.043	492	4.0	4.2	2.57	+0.42	0.0
	MRCI	1815.707 96	26.1	2.039	488	4.7	4.5	3.14	+0.46	0.0
	MRCI+Q	1815.712 1	26.8	2.041	484	4.6	4.6			0.0
	MRACPF	1815.710 82	26.6	2.041	485	4.5	4.5	3.20		0.0
	RCCSD(T)	1815.697 09	18.3	2.130	419	5.5	4.4			0.0
	MRCI(d^{10})	1816.138 1	24.5	1.983	510			2.56[e]	+0.39	0.0
	MRCI(d^{10})+Q	1816.176 5	24.9	1.975	499					0.0
	CASSCF/Rel	1832.016 44	19.8	2.031	502					
	MRCI/Rel	1832.105 18	25.2	2.027	474					
	MRCI+Q/Rel	1832.109 3	25.8	2.029	472					
	MRCI(d^{10})/Rel	1832.547 7	23.3	1.968	524					
	MRCI(d^{10})+Q/Rel	1832.587 6	23.7	1.960	513					
	QCISD(d^{10})[f]	1815.857 73		1.992	482.0			2.771		
	QCISD(T)(d^{10})[f]	1815.948 40[g]	21.3[g]							
	MRBWCCSD[h]	1815.696 23	20.8	2.096	460	6.7				
	MRBWCCSD(d^{10})[h]	1816.172 24	23.9	1.988						
$^5\Sigma^-(1)$	CASSCF	1815.593 55	73.7	2.004	559	2.9	3.4	1.55	+0.46	16.3
	MRCI	1815.675 14	83.9	2.006	553	3.1	3.5	2.07	+0.52	20.6
	MRCI+Q	1815.678 5	84.6	2.007	550	3.0	3.5			21.1
	MRCI(d^{10})	1816.102 64	88.7	1.948	575			1.45[e]	+0.43	22.3
	MRCI(d^{10})+Q	1816.138 5	89.3	1.918	601					23.8
	MRCI/Rel	1832.069 20	85.2	1.993	566					22.6
	MRCI+Q/Rel	1832.072 6	84.9	1.995	567					23.1
	MRCI(d^{10})/Rel	1832.508 62	90.1	1.933	596					24.5
	MRCI(d^{10})+Q/Rel	1832.545 7	90.4	1.925	586					26.3
	QCISD(d^{10})[f]	1815.827 970		1.942	587.0			1.749		18.7
	QCISD(T)(d^{10})[f]	1815.910 256[g]	85.3[g]							23.9
	MRBWCCSD[h]	1815.668 83	80.3	2.045	568	7.4				17.2
	MRBWCCSD(d^{10})[h]	1816.136 78	87.3	1.935						22.3
$^3\Pi(1)$	CASSCF	1815.584 48	0.01	5.819				−0.03	−0.00	22.0
	MRCI[i]	1815.666 55	0.2	4.33	24	2.3	6.5	−0.09	−0.00	26.0
	MRCI+Q[i]	1815.669 9	0.2	4.18	26	1.4	6.1			26.5
	MRCI(d^{10})[i]	1816.095 88	0.3	4.377	34			−0.11[e]	0.00	26.5
	MRCI(d^{10})+Q[i]	1816.136 2	0.4	4.16	27					25.3
	MRCI[j]	1815.666 56	0.2	2.28		2.1	2.2	0.65	+0.21	26.0
	MRCI +Q[j]	1815.671 4	1.2	2.27						25.5
	MRCI(d^{10})[j,k]									
	MRCI(d^{10})+Q[j]	1816.136 1	0.4	2.26						25.4
	QCISD(d^{10})[f]	1815.830 70		4.489	20.0			0.065		17.0
	QCISD(T)(d^{10})[f]	1815.914 730[g]	0.18[g]							21.1
$^1\Delta(1)$	CASSCF	1815.551 79	17.8	2.050	457	4.8	3.6	1.83	+0.21	42.5
	MRCI	1815.665 93	29.2	2.031	495	4.2	4.4	3.25	+0.41	26.4
	MRCI+Q	1815.673 8	31.2	2.034	494	4.0	4.3			24.0
	MRCI(d^{10})	1816.090 57	26.4	1.975	442			2.05[e]	+0.24	29.8
	MRCI(d^{10})+Q	1816.136 3	29.2	1.964	530					25.2
$^1\Pi(1)$	CASSCF	1815.557 31	18.0	2.144	451	3.2	3.6	1.53	+0.38	39.0
	MRCI	1815.649 90	19.1	2.153	435	3.7	3.9	1.66	+0.38	36.4
	MRCI+Q	1815.654 8	19.7	2.159	428	4.1	4.1			36.0
	MRCI(d^{10})	1816.074 77	17.3	2.123	439			0.94[e]	+0.22	39.8
	MRCI(d^{10})+Q	1816.118 4	18.6	2.106	428					36.4
$^1\Sigma^+(1)$	CASSCF	1815.537 63	8.4	2.054	448	4.4	3.4	1.69	+0.18	51.4
	MRCI	1815.644 13	15.4	2.038	491	4.1	4.5	3.11	+0.36	40.1
	MRCI+Q	1815.650 9	16.8	2.034	492	4.5	4.5			38.4
	MRCI(d^{10})	1816.070 8	13.9	1.969	522			1.98[e]	+0.21	42.2
	MRCI(d^{10})+Q	1816.114 5	15.5	1.957	519					38.9
$^3\Sigma^-(2)$	CASSCF	1815.516 13	38.2	2.025	608	15.1	9.8	1.73	+0.38	64.8
	MRCI	1815.622 42	51.8	2.029	530	8.7	6.7	2.63	+0.52	53.7
	MRCI+Q	1815.628 9	53.4	2.040	510	7.8	6.4			52.2
	MRCI(d^{10})	1816.045 24	53.6	1.961	536			1.84[e]	+0.41	58.3
	MRCI(d^{10})+Q	1816.086 2	56.7	1.957	528					56.7
$^3\Sigma^-(3)$	CASSCF	1815.475 82	13.1	2.457	354	3.3	1.7	−0.04	+0.08	90.1
	MRCI	1815.612 98	45.9	2.032	549	4.4	3.9	1.90	+0.49	59.6
	MRCI+Q	1815.620 1	47.9	2.062	515	4.5	5.2			57.7
	MRCI(d^{10})	1816.035 30	47.4	1.966	539			0.90[e]	+0.36	64.5
	MRCI(d^{10})+Q	1816.076 6	50.8	1.960	535					62.7
$^3\Delta(1)$	CASSCF	1815.496 96	26.3	2.055	475	4.2	4.6	0.46	+0.22	76.9
	MRCI	1815.612 36	45.4	2.041	510	3.5	3.8	1.98	+0.48	60.0
	MRCI+Q	1815.620 6	48.2	2.044	508	3.1	3.8			57.4
	MRCI(d^{10})	1816.030 85	44.5	1.973	497			1.05[e]	+0.31	67.3
	MRCI(d^{10})+Q	1816.075 2	49.8	1.959	492					63.6

TABLE 2: (Continued)

state[b]	method	$-E$	D_e[c]	r_e	ω_e	$\omega_e x_e$	α_e ($\times 10^{-3}$)	μ[d]	q_{Zn}	T_e
$^3\Pi(2)$	CASSCF	1815.502 26	29.5	1.895	637	10.2	10.5	3.26	+0.28	73.6
	MRCI	1815.609 24	43.5	1.891	670	14.3	19.2	4.47	+0.47	61.9
	MRCI+Q	1815.615 9	45.3	1.894	656	30.1	2.5			60.4
	MRCI(d^{10})	1816.033 22	46.1	1.823	688			3.52[e]	+0.31	65.8
	MRCI(d^{10})+Q	1816.075 7	50.2	1.810	696					63.2
	QCISD(d^{10})[f]	1815.757 037		1.821				4.184		63.2
	QCISD(T)(d^{10})[f]	1815.846 905[g]								63.7
$^1\Sigma^-(1)$	CASSCF	1815.494 15	23.4	2.087	428	4.3	5.0	1.30	+0.35	78.6
	MRCI	1815.603 02	39.4	2.086	456	3.6	4.1	2.33	+0.51	65.8
	MRCI+Q	1815.610 0	41.4	2.092	454	3.6	4.0			64.1
	MRCI(d^{10})	1816.022 43	38.8	2.014	480			1.53[e]	+0.39	72.6
	MRCI(d^{10})+Q	1816.064 6	42.9	2.007	429					70.2
$^3\Sigma^+(1)$	CASSCF	1815.483 24	17.5	2.116	385	1.5	5.1	−0.08	+0.16	85.5
	MRCI	1815.588 39	30.4	2.074	456	2.8	4.3	1.57	+0.40	75.0
	MRCI+Q	1815.595 5	32.4	2.074	468	3.9	4.1			73.2
	MRCI(d^{10})	1816.009 37	31.0	1.990	596			0.36[e]	+0.22	80.0
	MRCI(d^{10})+Q	1816.050 9	34.5	1.977	583					78.8
$^1\Sigma^+(2)$	CASSCF	1815.488 93	3.1	2.701	279	10.2	2.8	−1.87	−0.06	81.9
	MRCI	1815.586 51	12.0	2.631	335	5.6	1.2	−0.89	+0.02	76.2
	MRCI+Q	1815.592 8	13.4	2.628	336	5.2	0.6			74.9
	MRCI(d^{10})	1816.012 79	8.7	2.564	350			−1.85[e]	−0.07	78.6
	MRCI(d^{10})+Q	1816.054 1	10.8	2.539	346					76.8
$^1\Pi(2)$	CASSCF	1815.480 19	15.6	1.994	475	9.9	7.0	2.84	+0.57	87.4
	MRCI	1815.582 74	26.8	1.974	471	4.5	6.3	3.69	+0.56	78.5
	MRCI+Q	1815.589 7	28.8	1.975	473	5.0	5.9			76.8
	MRCI(d^{10})	1816.007 0	29.7	1.887	566			2.95[e]	+0.45	82.3
	MRCI(d^{10})+Q	1816.048 9	33.4	1.874	534					80.0
$^3\Pi(3)$	CASSCF	1815.461 03	3.7	2.418	368	17.2	2.1	−0.05	+0.14	99.4
	MRCI	1815.565 14	15.8	2.367	477	6.5	0.9	0.58	+0.24	89.6
	MRCI+Q	1815.572 8	18.3	2.358	479	2.8	0.9			87.4
	MRCI(d^{10})	1815.983 33	14.8	2.307	478			0.84[e]	+0.11	97.1
	MRCI(d^{10})+Q	1816.024 5	18.0	2.289	490					95.3
$^1\Delta(2)$	CASSCF	1815.466 27	8.0	2.729	235	3.7	2.1	−0.39	+0.00	96.1
	MRCI	1815.561 17	13.4	2.548	215	4.0	4.9	−0.34	−0.00	92.1
	MRCI+Q	1815.567 0	14.4	2.496	196	5.5	2.2			91.1
	MRCI(d^{10})	1815.982 50	14.7	2.477	244			−0.57[e]	−0.01	97.6
	MRCI(d^{10})+Q	1816.022 9	17.3	2.386	228					96.4
$^1\Sigma^-(2)$	CASSCF	1815.456 18	0.8	4.006	79	6.7	1.5	−0.07	+0.00	102.5
	MRCI	1815.558 76	11.9	2.322	304	5.0	4.8	−0.07	+0.04	93.6
	MRCI+Q	1815.566 1	14.1	2.318	325	5.9	3.2			91.6
	MRCI(d^{10})	1815.977 18	10.9	2.228	285			0.34[e]	+0.06	101.0
	MRCI(d^{10})+Q	1816.020 2	15.3	2.193	331					98.1
$^3\Delta(2)$	CASSCF	1815.443 95	28.6	2.269	376	2.8	3.3	0.56	+0.12	110.1
	MRCI	1815.552 06	37.0	2.267	352	4.2	4.3	0.28	+0.06	97.8
	MRCI+Q	1815.559 4	38.6	2.266	348	4.5	4.7			95.8
	MRCI(d^{10})	1815.972 12	38.2	2.195	381			0.04[e]	+0.04	104.2
	MRCI(d^{10})+Q	1816.015 0	41.3	2.177	371					101.3
$^1\Pi(3)$	CASSCF	1815.454 06	0.1	3.025				0.81	+0.09	103.8
	MRCI	1815.551 22	7.3	2.666	373	14.0	10.5	1.19	+0.19	98.4
	MRCI+Q	1815.557 6	8.7	2.642	384	12.4	9.5			97.0
	MRCI(d^{10})	1815.969 38	6.3	2.593	418			0.82[e]	+0.16	105.9
	MRCI(d^{10})+Q	1816.009 8	9.0	2.539	452					104.6
$^1\Sigma^+(3)$	CASSCF	1815.458 93	3.3	3.070	166	4.4	3.7	−0.32	−0.01	100.7
	MRCI	1815.548 45	5.5	2.909	160	3.2	4.7	−0.56	−0.03	100.1
	MRCI+Q	1815.553 7	6.0	2.776	148	2.3	1.2			99.4
	MRCI(d^{10})	1815.970 29	7.0	2.798	164			−0.51[e]	−0.02	105.3
	MRCI(d^{10})+Q	1816.008 8	8.4	2.710	179					105.2
$^5\Pi(1)$	MRCI	1815.547 23	4.4	2.111	355	14.0	10.5	1.66	+0.17	100.9
	MRCI+Q	1815.553 7	6.1	2.096	391	12.6	8.4			99.4
	MRCI(d^{10})	1815.968 68	5.2	2.045	340			1.00[e]	+0.07	106.3
	MRCI(d^{10})+Q	1815.008 0	7.5	2.023	438					105.7
$^3\Sigma^+(2)$	CASSCF	1815.435 48	23.4	2.240	407	2.8	2.6	0.61	+0.13	115.5
	MRCI	1815.545 82	33.1	2.239	389	2.4	3.1	0.70	+0.12	101.7
	MRCI+Q	1815.554 2	35.4	2.239	383	3.7	3.7			99.1
	MRCI(d^{10})	1815.962 55	31.9	2.159	351			0.09[e]	+0.06	110.1
	MRCI(d^{10})+Q	1816.006 5	35.7	2.112	259					106.7
$^5\Delta(1)$	CASSCF	1815.466 55	0.07	4.44				−0.15		96.0
	MRCI	1815.541 95	0.39	3.82				−0.35		104.2
	MRCI+Q	1815.545 08	0.45	3.8						104.8
	MRCI(d^{10})	1815.963 57	2.0	3.92				−0.40[e]		109.5
	MRCI(d^{10})+Q	1815.997 6	1.0	3.8						112.2
$^5\Sigma^-(2)$	CASSCF	1815.458 99	3.2	5.262				0.20	+0.01	100.7
	MRCI	1815.541 56	1.3	3.843				−0.35	−0.01	104.4
	MRCI+Q	1815.545 4	1.1	3.86						104.6

TABLE 2: (Continued)

state[b]	method	$-E$	D_e[c]	r_e	ω_e	$\omega_e x_e$	α_e ($\times 10^{-3}$)	μ[d]	q_{Zn}	T_e
$^5\Sigma^+(1)$	MRCI	1815.541 44	0.15	4.13						104.5
	MRCI+Q	1815.544 5	0.19	4.1						105.1
	MRCI(d^{10})	1815.963 10	1.74	4.30						109.8
	MRCI(d^{10})+Q	1815.997 0	0.59	4.0						112.6
$^5\Pi(2)$	repulsive									
$^3\Pi(4)$	CASSCF	1815.421 84	14.9	1.956	338	7.2	10.6	1.72	+0.27	124.0
	MRCI	1815.528 70	22.0	1.964	331	4.4	7.4	2.40	+0.40	112.5
	MRCI+Q	1815.537 0	24.2	1.982						109.9
	MRCI(d^{10})	1815.949 39	23.8	1.887				1.27[e]	+0.09	118.4
	MRCI(d^{10})+Q	1815.993 7	27.7	1.877						114.7
$^5\Sigma^-(3)$	MRCI	1815.515 98	0.9	3.94				0.32	+0.03	120.5
	MRCI+Q	1815.517 7	1.3	3.9						122.0
$^3\Pi(5)$	CASSCF[i]	1815.400 21	1.5	2.742	204	8.7	1.2	−0.70	−0.01	137.6
	MRCI[i]	1815.501 12	5.1	2.726				−1.33	−0.04	129.8
	MRCI+Q[i]	1815.508 3	6.6	2.671						127.9
	MRCI(d^{10})[i]	1815.919 43	5.1	2.354				0.27[e]	+0.09	137.2
	MRCI(d^{10})+Q[i]	1815.960 6	7.0	2.315						135.5
	CASSCF[j]	1815.402 63	3.0	2.315	550	6.3	9.0	0.38	+0.09	136.1
	MRCI[j]	1815.502 19	5.7	2.190	378	6.1	10.6	1.40	+0.19	129.1
	MRCI+Q[j]	1815.509 0	7.0	2.166	327	5.4	6.9			127.5
	MRCI(d^{10})[j]	1815.921 13	6.5	2.219	498			−0.31[e]	+0.08	136.2
	MRCI(d^{10})+Q[j]	1815.961 8	8.3	2.193	409					134.7
$^3\Delta(3)$	CASSCF	1815.398 01	0.13	5.78						139.0
	MRCI	1815.493 85	0.48	3.92						134.4
	MRCI+Q	1815.499 2	0.90	3.5						133.6

[a] Results with other methodologies for some states are also shown (see Table 1 for explanation of the acronyms). [b] Numbers in parentheses after the term symbol indicate the ordering according to energy, but within the same symmetry manifold. [c] Dissociation energy with respect to adiabatic products. [d] All dipole moments have been calculated as expectation values, $<\mu>$. For the X $^3\Sigma^-$ state the dipole moment obtained by the finite field approach at the MRCI(+Q) level is $\mu_{FF} = 3.17(3.22)$ D. [e] The much smaller $<\mu>$ value of the X $^3\Sigma^-$ state at the MRCI(d^{10}) level as compared to MRCI value, is rather due to severe nonextensivity errors; the corresponding finite field MRCI(d^{10})(+Q) value is $\mu_{FF} = 2.88(2.97)$ D. The same decrease of $<\mu>$ MRCI vs $<\mu>$ MRCI(d^{10}) was observed in all states (see also ref 27). [f] Quadratic Configuration Interaction, ref 15. [g] QCISD(T)(d^{10})//QCISD(d^{10}), ref 15. [h] Multireference Brillouin-Wigner coupled cluster singles and doubles, ref 8. [i] Local minimum at the MRCI level. [j] Global minimum at the MRCI level. [k] Unbound.

A qualitative view of the bonding can be envisaged using the valence-bond−Lewis (vbL) icon shown in eq 1, indicating

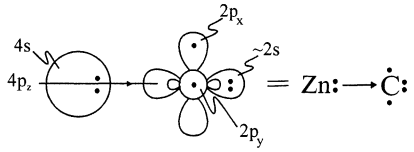

$$\mathrm{Zn}(^1\mathrm{S}) \quad \mathrm{C}(^3\mathrm{P};\ \mathrm{M_L}=0) \qquad \mathrm{X}^3\Sigma^- \tag{1}$$

that Zn and C are held by a σ "dative" bond amounting to 26.1 kcal/mol at the MRCI level ($r_e = 2.039$ Å). Including the $3d^{10}$ Zn e^- actually *decreases* the binding energy to 24.5 (24.9 at the MRCI+Q level) kcal/mol, 3.2 kcal/mol higher than the QCISD($3d^{10}$) result of Boldyrev and Simons,[15] however, reducing at the same time the quality of the wave function due to severe size nonextensivity errors. Douglas−Kroll relativistic effects further decrease the binding energy by 1.2 kcal/mol, bringing it to a final value of $D_e = 23.3$ (23.7 at the MRCI+Q level) kcal/mol. A similar trend is observed in bond lengths, where the 2.039 Å MRCI bond distance is reduced by $\delta r_e(d^{10}) = 0.056$ Å and $\delta r_e(DK) = 0.015$ Å, leading to a predicted $r_e = 1.968$ Å (1.960 at the +Q level). At equilibrium, about 0.5 e^- are transferred from Zn to C, almost all via the σ-frame. The two π electrons remain practically localized on C (Table 3 and eq 1).

The $^5\Sigma^-(1)$ state on the other hand is dominated by a single configuration at equilibrium (Table 3) and is adequately described by the following vbL scheme in eq 2. The Mulliken distributions show that the charge exchange is very similar to that in the X $^3\Sigma^-$ state (Table 3); the equilibrium charge on Zn is +0.46, the electrons being transferred mainly through the σ-frame and mainly from the $4p_z$ orbital. The second uncoupled σ electron and the two π electrons remain localized on the 4s

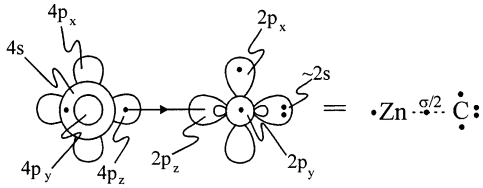

$$\mathrm{Zn}(^3\mathrm{P};\ \mathrm{M_L}=0) \quad \mathrm{C}(^3\mathrm{P};\ \mathrm{M_L}=0) \qquad {}^5\Sigma^-(1) \tag{2}$$

and 2p orbitals of Zn and C, respectively. The binding energy for this high-spin state is indeed large, $D_e = 83.9$ kcal/mol at the MRCI level [89.3 at the MRCI(d^{10})+Q level], or 85.2 (90.4) including relativistic effects, in practical agreement with the QCISD(d^{10}) results of Boldyrev and Simons.[15] Here, the $3d^{10}$ electrons increase the binding energy by about 5 kcal/mol, while the bond length is again shortened by ~0.06 Å. The large difference in the binding energies between the X $^3\Sigma^-$ and the $^5\Sigma^-(1)$ states can be interpreted by remembering the in situ excited ^{3}P ($4s^14p^1$) character of Zn in the $^5\Sigma^-$ state, which proves to be very effective in binding (see the PECs in Figure 1) due to the bonding availability of the 4p orbitals (vide infra) and the much larger participation of the 2s orbital of C in $2s2p_z$ hybridization (Table 3).

At the MRCI [MRCI(d^{10})+Q] level we predict the energy separation T_e ($^5\Sigma^-(1) \leftarrow X^3\Sigma^-$) = 20.6 (23.8) kcal/mol, or 22.6 (26.3) including DK-relativistic effects, in agreement with the final values of Kerkines et al.[8] and with the QCISD(d^{10}) results of Boldyrev and Simons.[15] For the isovalent CaC system, the same T_e was calculated to be at least 4.2 kcal/mol, even though

TABLE 3: Asymptotic Fragments, Leading Equilibrium CASSCF CFs, and Equilibrium CASSCF Mulliken Atomic Populations of 26 ZnC Bound States Studied

			equilibrium CASSCF Mulliken atomic populations							
			Zn				C			
state	asymptotic fragments	leading equilibrium CASSCF CFs	4s	$4p_z$	$4p_x$	$4p_y$	2s	$2p_z$	$2p_x$	$2p_y$
$X\ ^3\Sigma^-$	$\|0\rangle\|0\rangle^a$	$0.89\|1\sigma^2 2\sigma^2 1\pi_x^1 1\pi_y^1\rangle - 0.31\|1\sigma^2 3\sigma^2 1\pi_x^1 1\pi_y^1\rangle$	1.26	0.22	0.04	0.04	1.79	0.71	0.95	0.95
$^5\Sigma^-(1)$	$\|0\rangle\|0\rangle^c$	$0.98\|1\sigma^2 2\sigma^1 3\sigma^1 1\pi_x^1 1\pi_y^1\rangle$	0.98	0.43	0.05	0.05	1.68	0.89	0.94	0.94
$^3\Pi(1)$	$\|0\rangle\|\pm1\rangle^a$	$0.95\|1\sigma^2 2\sigma^2 3\sigma^1 1\pi_x^1\rangle^{g,i}$	1.55	0.23	0.06	0.02	1.89	1.21	0.96	0.06
$^1\Delta(1)$	$\|0\rangle\|\pm2\rangle^b$	$0.64(\|1\sigma^2 2\sigma^2 1\pi_x^2\rangle - \|1\sigma^2 2\sigma^2 1\pi_y^2\rangle)^h$	1.28	0.12	0.20	0.20	1.83	0.73	0.81	0.81
$^1\Pi(1)$	$\|0\rangle\|\pm1\rangle^b$	$0.68(\|1\sigma^2 2\sigma^2 3\sigma^1 1\pi_x^1\rangle - \|1\sigma^2 2\sigma^2 3\sigma^1 1\bar{\pi}_x^1\rangle)^g$	1.12	0.49	0.02	0.00	1.89	1.39	0.97	0.08
$^1\Sigma^+(1)$	$\|0\rangle\|0\rangle^b$	$0.62(\|1\sigma^2 2\sigma^2 1\pi_x^2\rangle + \|1\sigma^2 2\sigma^2 1\pi_y^2\rangle)$	1.24	0.10	0.25	0.25	1.80	0.78	0.78	0.78
$^3\Sigma^-(2)$	$\|0\rangle\|0\rangle^c$	$0.73\|1\sigma^2 2\sigma^1 3\sigma^1 1\bar{\pi}_x^1 1\pi_y^1\rangle + 0.52\|1\sigma^2 2\sigma^1 3\sigma^1 1\pi_x^1 1\bar{\pi}_y^1\rangle$	0.96	0.41	0.13	0.13	1.76	0.85	0.87	0.87
$^3\Sigma^-(3)$	$\|\pm1\rangle\|\mp1\rangle^c$	$0.66\|1\sigma^2 2\sigma^1 3\bar{\sigma}^1 1\pi_x^1 1\pi_y^1\rangle - 0.40(\|1\sigma^2 2\sigma^2 2\pi_x^1 1\pi_y^1\rangle + \|1\sigma^2 2\sigma^2 1\pi_x^1 2\pi_y^1\rangle)$	1.07	0.21	0.25	0.25	1.85	0.80	0.76	0.76
$^3\Delta(1)$	$\|\pm1\rangle\|\pm1\rangle^c$	$0.64(\|1\sigma^2 2\sigma^1 3\sigma^1 1\pi_y^2\rangle - \|1\sigma^2 2\sigma^1 3\sigma^1 1\pi_x^2\rangle)^h$	1.00	0.32	0.23	0.23	1.77	0.88	0.77	0.77
$^3\Pi(2)$	$\|\pm1\rangle\|0\rangle^c$	$0.86\|1\sigma^2 2\sigma^1 1\pi_x^1 1\pi_y^2\rangle^g$	0.81	0.11	0.14	0.68	1.60	0.51	0.86	1.28
$^1\Sigma^-(1)$	$\|0\rangle\|0\rangle^c$	$0.89\|1\sigma^2 2\sigma^1 3\sigma^1 1\bar{\pi}_x^1 1\bar{\pi}_y^1\rangle$	0.92	0.40	0.16	0.16	1.82	0.84	0.83	0.83
$^3\Sigma^+(1)$	$\|\pm1\rangle\|\mp1\rangle^c$	$0.60(\|1\sigma^2 2\sigma^1 3\sigma^1 2\pi_x^2\rangle + \|1\sigma^2 2\sigma^1 3\sigma^1 1\pi_x^2\rangle)$	0.98	0.27	0.29	0.29	1.78	0.90	0.72	0.72
$^1\Sigma^+(2)$	$\|0\rangle\|0\rangle^d$	$0.81\|1\sigma^2 2\sigma^2 3\sigma^2\rangle + 0.23(\|1\sigma^2 2\sigma^2 1\pi_y^2\rangle + \|1\sigma^2 2\sigma^2 1\pi_x^1\rangle)$	1.72	0.08	0.13	0.13	1.86	1.64	0.21	0.21
$^1\Pi(2)$	$\|0\rangle\|\pm1\rangle^c$	$0.85\|1\sigma^2 2\sigma^1 1\bar{\pi}_x^1 1\pi_y^2\rangle - 0.38\|1\sigma^2 3\sigma^1 1\bar{\pi}_x^1 1\pi_y^2\rangle^g$	0.90	0.23	0.06	0.21	1.75	0.17	0.93	1.67
$^3\Pi(3)$	$\|0\rangle\|\pm1\rangle^c$	$0.77\|1\sigma^2 2\sigma^1 3\sigma^2 1\pi_x^1\rangle + 0.32\|1\sigma^2 2\sigma^1 1\pi_x^1 1\pi_y^2\rangle^g$	1.17	0.35	0.15	0.20	1.85	1.08	0.87	0.31
$^1\Sigma^+(3)$	$\|\pm1\rangle\|\mp1\rangle^c$	$0.37(\|1\sigma^2 2\sigma^2 1\pi_x^1 2\bar{\pi}_x^1\rangle + \|1\sigma^2 2\sigma^2 1\pi_y^1 2\bar{\pi}_y^1\rangle) + 0.33(\|1\sigma^2 2\sigma^1 3\bar{\sigma}^1 1\pi_x^1 2\bar{\pi}_x^1\rangle + \|1\sigma^2 2\sigma^1 3\bar{\sigma}^1 1\pi_y^1 2\bar{\pi}_y^1\rangle) - 0.28(\|1\sigma^2 2\sigma^1 3\bar{\sigma}^1 1\pi_x^2\rangle + \|1\sigma^2 2\sigma^1 3\bar{\sigma}^1 1\pi_y^2\rangle) + 0.28(\|1\sigma^2 2\sigma^1 3\sigma^1 1\bar{\pi}_x^1 2\bar{\pi}_x^1\rangle + \|1\sigma^2 2\sigma^1 3\sigma^1 1\bar{\pi}_y^1 2\bar{\pi}_y^1\rangle)$	1.23	0.02	0.38	0.38	1.90	0.83	0.62	0.62
$^1\Sigma^-(2)$	$\|\pm1\rangle\|\mp1\rangle^c$	$0.52(\|1\sigma^2 2\sigma^1 3\sigma^1 1\bar{\pi}_x^1 1\bar{\pi}_y^1\rangle - \|1\sigma^2 2\sigma^2 2\pi_x^1 1\bar{\pi}_y^1\rangle + \|1\sigma^2 2\sigma^2 1\pi_x^1 2\bar{\pi}_y^1\rangle)$	0.95	0.24	0.31	0.31	1.90	0.86	0.70	0.70
$^3\Delta(2)$	$\|\pm1\rangle\|\pm1\rangle^e$	$0.58(\|1\sigma^2 2\sigma^2 1\pi_y^1 2\pi_y^1\rangle - \|1\sigma^2 2\sigma^2 1\pi_x^1 2\pi_x^1\rangle) + 0.30(\|1\sigma^2 2\sigma^1 3\sigma^1 1\pi_x^2\rangle - \|1\sigma^2 2\sigma^1 3\sigma^1 1\pi_y^2\rangle)^h$	0.96	0.13	0.39	0.39	1.89	0.96	0.62	0.62
$^1\Pi(3)$	$\|\pm1\rangle\|0\rangle^c$	$0.71\|1\sigma^2 2\sigma^1 3\sigma^2 1\bar{\pi}_x^1\rangle + 0.35\|1\sigma^2 2\sigma^2 4\sigma^1 1\bar{\pi}_x^1\rangle^g$	1.24	0.45	0.03	0.16	1.91	0.95	0.99	0.25
$^1\Delta(2)$	$\|\pm1\rangle\|\pm1\rangle^c$	$0.44(\|1\sigma^2 2\sigma^2 1\pi_x^1 2\bar{\pi}_x^1\rangle - \|1\sigma^2 2\sigma^2 1\pi_y^1 2\bar{\pi}_y^1\rangle) - 0.34(\|1\sigma^2 2\sigma^1 3\bar{\sigma}^1 1\pi_x^2\rangle - \|1\sigma^2 2\sigma^1 3\bar{\sigma}^1 1\pi_y^2\rangle)^h$	1.22	0.03	0.37	0.37	1.91	0.77	0.65	0.65
$^5\Pi(1)$	$\|\pm1\rangle\|0\rangle^c$	$0.98\|1\sigma^2 2\sigma^1 1\pi_x^1 1\pi_y^1 2\pi_y^1\rangle^g$	0.82	0.07	0.05	1.04	1.69	0.41	0.94	0.96
$^3\Sigma^+(2)$	$\|\pm1\rangle\|\mp1\rangle^e$	$-0.55(\|1\sigma^2 2\sigma^2 1\pi_x^1 1\pi_y^1\rangle + \|1\sigma^2 2\sigma^2 2\pi_x^1 2\pi_y^1\rangle) + 0.35(\|1\sigma^2 2\sigma^1 3\sigma^1 1\pi_x^2\rangle + \|1\sigma^2 2\sigma^1 3\sigma^1 2\pi_x^2\rangle)$	0.96	0.14	0.38	0.38	1.87	0.96	0.64	0.64
$^5\Sigma^-(2)$	$\|\pm1\rangle\|\mp1\rangle^c$	$0.65(\|1\sigma^2 2\sigma^1 3\sigma^1 2\pi_x^1 1\pi_y^1\rangle + \|1\sigma^2 2\sigma^1 3\sigma^1 1\pi_x^1 2\pi_y^1\rangle) + 0.34\|1\sigma^2 2\sigma^1 4\sigma^1 1\pi_x^1 1\pi_y^1\rangle$	1.00	0.12	0.44	0.44	1.95	0.88	0.58	0.58
$^3\Pi(4)$	$\|\pm1\rangle\|0\rangle^e$	$-0.67\|1\sigma^2 3\sigma^1 1\pi_x^1 1\pi_y^2\rangle + 0.47\|1\sigma^2 2\sigma^1 1\pi_x^1 1\pi_y^1 2\bar{\pi}_y^1\rangle - 0.24\|1\sigma^1 2\sigma^2 1\pi_x^1 1\pi_y^2\rangle + 0.23\|1\sigma^2 3\sigma^1 1\pi_x^1 1\pi_y^1 2\bar{\pi}_y^1\rangle^g$	0.74	0.23	0.11	0.66	1.52	0.56	0.90	1.27
$^5\Sigma^-(3)$	$\|0\rangle\|0\rangle^f$	$0.87\|1\sigma^2 2\sigma^1 4\sigma^1 1\pi_x^1 2\pi_x^1\rangle - 0.27\|1\sigma^2 2\sigma^1 3\sigma^1 1\pi_x^1 2\pi_x^1\rangle + 0.24(\|1\sigma^2 2\sigma^1 3\sigma^1 1\pi_y^1 2\pi_x^1\rangle + \|1\sigma^2 2\sigma^1 3\sigma^1 1\pi_x^1 2\pi_y^1\rangle)$	1.06	0.74	0.09	0.09	1.88	0.30	0.92	0.92
$^3\Pi(5)$	$\|0\rangle\|\pm1\rangle^e$	$-0.46\|1\sigma^2 2\sigma^1 3\sigma^2 2\pi_x^1\rangle - 0.40\|1\sigma^2 2\sigma^1 1\bar{\pi}_x^1 1\pi_y^1 2\pi_y^1\rangle + 0.39\|1\sigma^2 2\sigma^1 1\pi_x^2 2\pi_x^1\rangle + 0.37\|1\sigma^2 2\sigma^2 3\sigma^1 2\bar{\pi}_x^1\rangle + 0.28\|1\sigma^2 2\sigma^1 1\pi_x^1 1\pi_y^2\rangle + 0.27\|1\sigma^2 2\sigma^1 1\pi_x^1 1\bar{\pi}_y^1 2\pi_y^1\rangle^{g,i}$	1.00	0.07	0.63	0.30	1.92	0.80	0.70	0.56
		$0.69\|1\sigma^2 2\sigma^1 1\bar{\pi}_x^1 1\pi_y^1 2\pi_y^1\rangle + 0.44\|1\sigma^2 2\sigma^1 2\pi_x^1 1\pi_y^2\rangle - 0.25\|1\sigma^2 2\sigma^1 1\pi_x^1 1\pi_y^2\rangle^{g,j}$	0.84	0.06	0.32	0.70	1.83	0.28	0.71	1.23

[a] $|Zn,^1S;M_L\rangle|C,^3P;M_L\rangle$. [b] $|Zn,^1S;M_L\rangle|C,^1D;M_L\rangle$. [c] $|Zn,^3P;M_L\rangle|C,^3P;M_L\rangle$. [d] $|Zn,^1S;M_L\rangle|C,^1S;M_L\rangle$. [e] $|Zn,^3P;M_L\rangle|C,^1D;M_L\rangle$. [f] $|Zn,^1S;M_L\rangle|C,^5S;M_L\rangle$. [g] B_1 symmetry component. [h] A_1 symmetry component. [i] Global minimum at the MRCI level. [j] Local minimum at the MRCI level.

the CaC $X\ ^3\Sigma^-$ potential energy well is almost twice as deep (51.1 kcal/mol).[7]

Zn(^{1}S) + C(^{3}P) Channel. Apart from the $X\ ^3\Sigma^-(1)$ state, this channel produces also the $^3\Pi(1)$ state, referring to the approach of C to Zn via its $M_L = \pm1$ component (eq 3). As

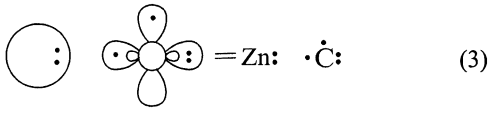

$$\mathrm{Zn}(^1\mathrm{S}) \quad \mathrm{C}(^3\mathrm{P};\ M_L=\pm1) \quad ^3\Pi(1) \tag{3}$$

expected from the electron distribution along the σ-frame, this state should be essentially repulsive. Boldyrev and Simons[15] have found a long-range van der Waals minimum of 0.18 kcal/mol at $r_e = 4.489$ Å. At the MRCI level we find a similar minimum at $r_e = 4.33$ Å (~8.2 bohr) with a depth of 0.2 kcal/mol. In addition, there proves to be a second short-range and "formally global" minimum of the same magnitude at 2.28 Å (~4.3 bohr) (Table 2). A look at the wave function composition and Mulliken charge distributions (Table 3) indicates significant $4s4p_z$ hybridization on Zn, allowing a small (~0.1 e^-) electron charge transfer to C along the σ-frame, resulting in a relatively sizable dipole moment of 0.65 D (Table 2).

The $^3\Pi(1)$ curve suffers an avoided crossing with the $^3\Pi(2)$ state correlating adiabatically to the Zn(^{3}P) + C(^{3}P) fragments at its repulsive part. A better view of the crossing can be seen

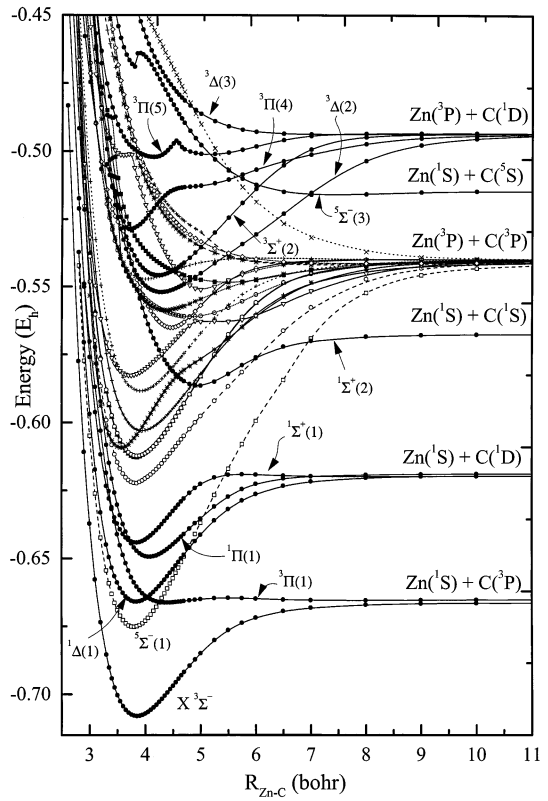

Figure 1. Potential energy curves of all 30 states of the ZnC molecule at the MRCI level of theory.

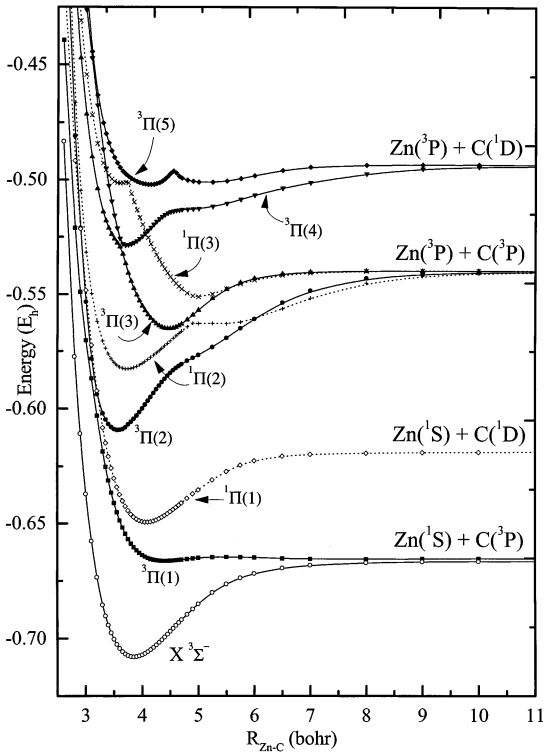

Figure 2. Potential energy curves of the $^3\Pi$ and $^1\Pi$ states of the ZnC system at the MRCI level of theory.

in Figure 2, where the avoided crossings of five $^3\Pi$ and three $^1\Pi$ states are shown.

Zn(^{1}S) + C(^{1}D) and Zn(^{1}S) + C(^{1}S) Channels. Three states emerge from the first channel, $^1\Sigma^+(1)$, $^1\Pi(1)$, and $^1\Delta(1)$, corresponding respectively to the three different ways (M_L = 0, ±1, and ±2, respectively) that C(^{1}D) can approach the closed-shell Zn(^{1}S) atom. In addition, a single $^1\Sigma^+(2)$ state is produced from the second channel. As seen in Figure 1 and Table 2, the ordering according to decreasing binding energy among the first three states is (in kcal/mol) $^1\Delta(1)$ (29.2) > $^1\Pi(1)$ (19.1) > $^1\Sigma^+(1)$ (15.4), reflecting the orbital composition of each M_L state of C (±2, ±1, and 0, respectively). Specifically, the M_L = 0 (Σ^+) component of C(^{1}D) has the composition $(2/\sqrt{6})(p_z^2) - (1/\sqrt{6})(p_x^2 + p_y^2)$, while the $M_L = \pm 2$ (Δ) component is $(1/\sqrt{2})(p_x^2 - p_y^2)$ in A_1 symmetry and $(1/\sqrt{2})(p_x\bar{p}_y - p_y\bar{p}_x)$ in A_2 symmetry. The $(2/\sqrt{6})(p_z^2)$ term of the $M_L = 0$ component obstructs bond formation; thus, upon the mutual approach of the Zn and C atoms, this term becomes gradually transferred to the $^1\Sigma^+(2)$ state coming from the Zn(^{1}S) + C(^{1}S) channel as a result of an interaction between $^1\Sigma^+(1)$ and $^1\Sigma^+(2)$ (Figure 1). Apparently, this crossing causes the small "hump" in the PEC of the $^1\Sigma^+(1)$ state near 5.5 bohr. The (p_z^2) term is practically absent in the equilibrium of the $^1\Delta(1)$ state; thus, bond formation is easier, leading to a much larger well than that in the $^1\Sigma^+(1)$ state. A qualitative picture of the bonding situation for both $^1\Delta(1)$ and $^1\Sigma^+(1)$ states in equilibrium is shown in eq 4.

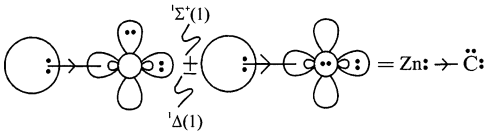

(4)

$Zn(^1S) + C(^1D; M_L=0 \text{ or } 2)$ $^1\Sigma^+(1)$ or $^1\Delta(1)$

Apart from the difference in binding energy, 13.8 kcal/mol, all other parameters including spectroscopic constants, dipole moments, and atomic populations are very similar in both states. The 4s orbital of Zn is significantly hybridized, while the $2p_z$ orbital of C now carries more than 0.7 e^- (Table 3).

On the other hand, the $^1\Sigma^+(2)$ state starting at infinity with equal weights, $(1/\sqrt{3})|1\sigma^2 2\sigma^2(3\sigma^2 + 1\pi_x^2 + 1\pi_y^2)\rangle$ changes its character as the two atoms approach due to the aforementioned interaction with the $^1\Sigma^+(1)$ state, and thus, a rather weak (12.0 kcal/mol) bond is formed at a rather large interatomic distance, 2.631 Å (Table 3). Including the $3d^{10}$ electrons reduces the binding energy to 10.8 kcal/mol [MRCI(d^{10})+Q level]. Although a small 4s4p and 2s2p hybridization is noted, there is almost no net charge transfer between Zn and C. At its repulsive part, the $^1\Sigma^+(2)$ state undergoes an avoided crossing at around 3.9 bohr with the $^1\Sigma^+(3)$ state correlating adiabatically to Zn(^{3}P; $M_L = \pm 1$) + C(^{3}P; $M_L = \mp 1$).

Finally, the $^1\Pi(1)$ state is represented at infinity by the wave function $(1/\sqrt{2})|1\sigma^2 2\sigma^2(3\sigma^1 1\bar{\pi}_x^1 + 3\bar{\sigma}^1 1\pi_x^1)\rangle$; as seen from Table 3, this character is practically retained at equilibrium. Although the π electron is localized on C, the bonding situation along the σ-frame proves rather involved, as seen from the atomic orbital composition of the 2σ and 3σ MOs at equilibrium:

$$2\sigma = -0.93(4s)_{Zn} + 0.29(2p_z)_C$$

$$3\sigma = 0.43(4s)_{Zn} + 0.82(2p_z)_C - 0.35(4p_z)_{Zn}$$

According to the Mulliken populations, the 4s orbital has transferred a significant amount of its electronic charge to the $2p_z$ orbital through the $4p_z$ orbital, which at equilibrium carries about half an electron; overall, C acquires ~0.4 e^- from Zn. It should also be noted that our CASSCF binding energy is 18.0 kcal/mol, only ~1 kcal/mol lower than the MRCI result.

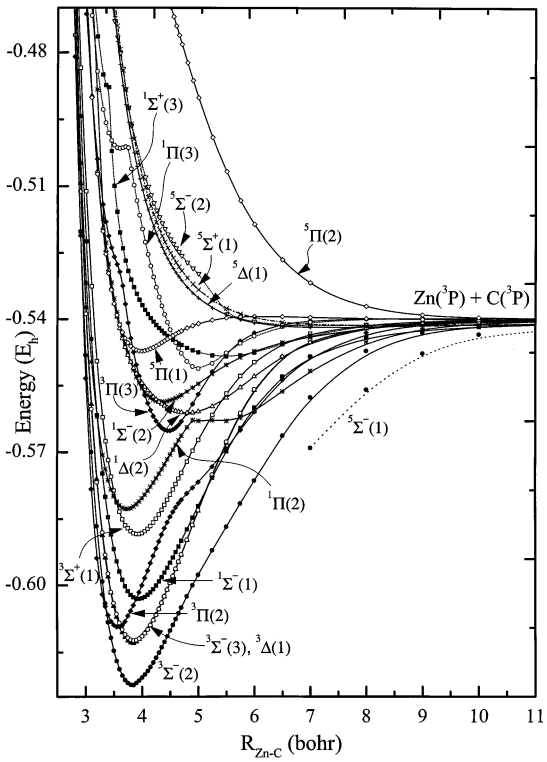

Figure 3. Potential energy curves of ZnC at the MRCI level which stem from the Zn(^{3}P) and C(^{3}P) channel.

Zn(^{3}P) + C(^{3}P) Channel. Eighteen states trace their lineage to this channel (Figure 3). Apart from the already mentioned $^5\Sigma^-(1)$ state, we find a state bearing the same symmetry as the ground state, $^3\Sigma^-(2)$, lying 53.7 kcal/mol [56.7 at the MRCI-(d^{10})+Q level] above the X $^3\Sigma^-$ state. Although this state originates from the (0,0) M_L components, near 5 bohr it undergoes an avoided crossing with the incoming $^3\Sigma^-(3)$ state originating from the ($\pm1,\mp1$) M_L components and being 59.6 [62.7 at the MRCI(d^{10})+Q level] kcal/mol above the X $^3\Sigma^-$ state. The bonding in these two states *in equilibrium* is captured qualitatively by the vbL icons in eq 5 and 6.

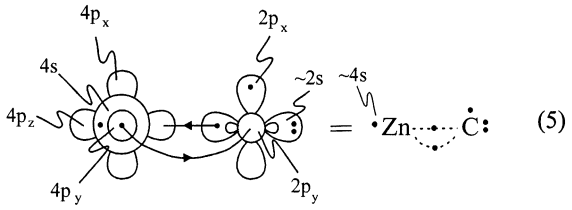

(5)

$Zn(^3P; M_L=\pm1)$ $C(^3P; M_L=\mp1)$ $^3\Sigma^-(2)$

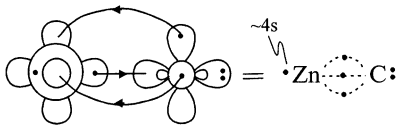

(6)

$Zn(^3P; M_L=0)$ $C(^3P; M_L=0)$ $^3\Sigma^-(3)$

From Table 3 it is obvious that the 4s electron remains localized on Zn in both states. Meanwhile, in the $^3\Sigma^-(2)$ state, Zn transfers ~0.7 e$^-$ to C via the π-frame, receiving back ~0.35 e$^-$ via the σ-system, essentially to its 4p$_z$ orbital. A similar charge exchange is observed in the $^3\Sigma^-(3)$ state, but this time Zn becomes the σ-donor and π-acceptor. These two states are strongly bound with respect to their asymptotic products: 51.8 (56.7) and 45.9 (50.8) kcal/mol at the MRCI [MRCI(d^{10})+Q] level of theory, at bond distances similar to those for the X $^3\Sigma^-$ state.

The $^3\Delta(1)$ state ensuing from the ($\pm1,\pm1$) M_L combination of this dissociation channel has a strikingly similar PEC to that of the $^3\Sigma^-(3)$ state (Figure 3). The bonding is captured by the vbL icon in eq 7. The bonding similarities with the $^3\Sigma^-(3)$ state

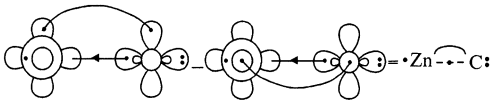

(7)

$Zn(^3P; M_L=\pm1) + C(^3P; M_L=\pm1)$ $^3\Delta(1)$

apparently arise from the $2\sigma^1 3\sigma^1 1\pi^2$ configuration common in both states (Table 3). Indeed, the Mulliken population distributions, energies, and spectroscopic parameters are practically identical (Tables 2 and 3). The vbL icon in eq 7, but with a "+" sign, describes the $^3\Sigma^+(1)$ state, a state which, as shown from Table 3, has the same charge distribution as both $^3\Sigma^-(3)$ and $^3\Delta(1)$ states but a weaker and longer bond, as shown in Table 2. As a result, the $^3\Sigma^+(1)$ state lies about 15 kcal/mol higher than the $^3\Delta(1)$ state. Note that, again, the 4s orbital carries practically 1.0 e$^-$ along all three PECs.

We could think of the $^1\Sigma^-(1)$ state (Figure 3) arising from the same $2\sigma^1 3\sigma^1 1\pi^2$ configuration, but with the four electrons singlet coupled; thus, the bond is also adequately described by the vbL icon in eq 6. This is corroborated by the very similar electron distribution as compared with the aforementioned $^3\Sigma^-(2)$, $^3\Sigma^-(3)$, and $^3\Delta(1)$ states. The minimum of the $^1\Sigma^-(1)$ state lies 65.8 (70.2) kcal/mol above the X $^3\Sigma^-$ state, having a binding energy of 39.4 (42.9) kcal/mol with respect to its asymptotic channel at the MRCI [MRCI(d^{10})+Q] level of theory. The same leading configuration is found in the $^1\Sigma^-(2)$ state, located 93.6 (98.1) kcal/mol above the ground state at the MRCI [MRCI(d^{10})+Q] level of theory, though at about 0.2 Å longer equilibrium interatomic distance. A σ electron is again localized on the 4s orbital of Zn (Table 3), but the charge exchange in this case is much less than that in the aforementioned states, leading to an almost zero dipole moment and a binding energy of only 11.9 (15.3) kcal/mol (Table 2).

The $^3\Pi(2)$ state, lying 61.9 (63.2) kcal/mol above the X $^3\Sigma^-$ state at the MRCI [MRCI(d^{10})+Q] level shows some interesting features. It is the state with the shortest bond length, 1.891 (1.810) Å, even shorter than that of the ground state by 0.15 (0.17) Å (Table 2). We can see why by looking at its vbL icon (B_1 component, eq 8).

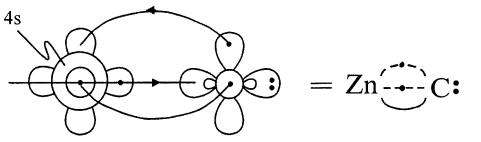

(8)

$Zn(^3P; M_L=\pm1)$ $C(^3P; M_L=0)$ $^3\Pi(2)$

The $^3\Pi(2)$ state starts at infinity as a combination of the (0,±1) M_L components of the Zn(^{3}P) + C(^{3}P) states. At around 4.7 bohr though, an avoided crossing with the $^3\Pi(3)$ state is observed (Figure 2), a state which also correlates to Zn(^{3}P) + C(^{3}P), but with M_L= (±1,0). As seen from eq 8, the Zn and C atoms are held together by what is essentially a "double" bond ((1/2)σ and ~(3/2)π), leading to a very small bond length and a binding energy of 43.5 (50.2) kcal/mol at the MRCI [MRCI-(d^{10})+Q] level of theory (Table 2). As mentioned before, the $^3\Pi(2)$ state interacts strongly with the $^3\Pi(1)$ state at their

repulsive parts (~3.1 bohr, Figure 2). An overall transfer of 0.3 e^- from Zn to C is observed, practically shared equally by the σ and π skeletons of the system. At the MRCI level the predicted dipole moment is 4.47 D, close to the one obtained by Boldyrev and Simons, 4.184 D at the QCISD level (Table 2).[15]

A state with similar but much less pronounced characteristics is obtained by a spin flip of the unpaired π electron, the $^1\Pi(2)$ state, 78.5 (80.0) kcal/mol above the ground state (Table 2). As seen in Figure 2, near 5 bohr, we encounter a similar $^1\Pi(2)-{}^1\Pi(3)$ avoided crossing due to the exchange of the (±1,0) and (0,±1) M_L values of Zn(^{3}P) and C(^{3}P), respectively. Like the $^3\Pi(2)$ state, the $^1\Pi(2)$ state has a short bond length, 1.974 Å, and a binding energy of 26.8 kcal/mol (MRCI, Table 2). The Mulliken distributions show that almost 0.6 e^- are transferred from Zn to C via both σ and π frames (Table 3). Finally, we also find a second avoided crossing at the repulsive part of the PEC between the $^1\Pi(2)$ and $^1\Pi(1)$ PECs (Figure 2).

The resemblance between the singlet and triplet Π states continues in the case of the $^3\Pi(3)$ and $^1\Pi(3)$ states, as is clearly shown in Figure 2. Although the $^3\Pi(3)$ state has a larger well (15.8 vs 7.3 kcal/mol) at a shorter distance (2.367 vs 2.666 Å), the morphology of the two PECs is the same, undergoing two avoided crossings at similar distances: one already mentioned, with the $^3\Pi(2)$ and $^1\Pi(2)$ states near 5 bohr, and a second one at their repulsive parts (~4 bohr) with the $^3\Pi(4)$ and the (not calculated) $^1\Pi(4)$ states correlating asymptotically to the higher Zn(^{3}P) + C(^{1}D) channel (Figure 2). From Table 3 we note that the CASSCF Mulliken populations and the dominant configurations are practically the same, save the spin flip of the unpaired π electron to satisfy the spin symmetry of the $^1\Pi(3)$ state. Certain features of the bonding can be condensed in the vbL icon in eq 9. In both states the 2σ orbital is essentially a Zn 4s

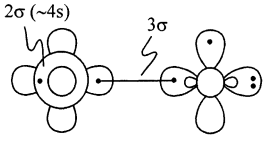

$$= \cdot Zn - \dot{C}: \qquad (9)$$

$Zn(^3P; M_L=0)$ $C(^3P; M_L=\pm1)$ $^{1,3}\Pi(3)$

function with a small $4p_z$ participation. The doubly occupied 3σ orbital has the following composition:

$$3\sigma \sim 0.70(4s) - 0.25(4p_z) + 0.78(2p_z) \quad (^3\Pi(3))$$

and

$$3\sigma \sim 0.75(4s) - 0.49(4p_z) + 0.52(2p_z) \quad (^1\Pi(3))$$

The charge distribution (Table 3) shows that C carries more than 1 e^- in its p_π orbitals, indicating the active participation of other CFs affecting the bonding.

The $^1\Delta(2)$ and $^1\Sigma^+(3)$ states located 92.1 (96.4) and 100.1 (105.2) kcal/mol above the X $^3\Sigma^-$ state at the MRCI [MRCI-(d^{10})+Q] level are described by a similar linear combination of CFs but with a different sign with which the CFs participate ("+" for the Σ^+ state and "−" for the Δ state) (Table 3). The CASSCF atomic populations are nearly identical, indicating a ~0.25 e^- Zn-to-C transfer via the π-frame, with a roughly similar back-donation via the σ-frame practically to the 4s Zn orbital. As a result, hardly any charge transfer is observed between the two atoms, in accordance with the small MRCI dipole moments of −0.56 D [$^1\Sigma^+(3)$] and −0.34 D [$^1\Delta(2)$]. Notice the minus sign of the dipole moment in both states, indicating the negative Zn end of the molecule. The highly complicated multireference character observed (Table 3) prevents us from drawing a consistent vbL icon for these two particular states.

The five remaining states emerging from the Zn(^{3}P) + C(^{3}P) channel are all quintets, that is, $^5\Sigma^-(2)$, $^5\Pi(1)$, $^5\Delta(1)$, $^5\Sigma^+(1)$, and $^5\Pi(2)$ in ascending energy order (Figure 3). Only the $^5\Pi(1)$ state shows an appreciable potential energy well of 4.4 (7.5) kcal/mol at a bond distance of 2.111 (2.023) Å at the MRCI [MRCI(d^{10})+Q] level. The other four quintets are essentially repulsive with weak van der Waals minima at large interatomic distances (Table 2). The bound $^5\Pi(1)$ state lies 100.9 (105.7) kcal/mol above the ground state and, as seen from Table 3, is dominated by the configuration $1\sigma^2 2\sigma^1 1\pi_x^1 1\pi_y^1 2\pi_y^1$ (B_1 component). The bonding scenario leading to this state can be captured following the vbL icon in eq 10.

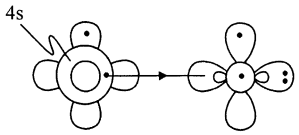

$$= \dot{Z}n \text{-} \cdot \text{-} \dot{C}: \qquad (10)$$

$Zn(^3P; M_L=\pm1)$ $C(^3P; M_L=0)$ $^5\Pi(1)$

The π electrons remain localized on Zn and C, with negligible charge transfer via the σ-frame from Zn to C. It should be noted that the binding energy in this state is all due to "dynamical" correlation energy; indeed, at the CASSCF level, the PEC is repulsive.

Zn(^{1}S) + C(^{5}S) and Zn(^{3}P) + C(^{1}D) Channels. A single $^5\Sigma^-$ ZnC state originates from the former, and nine triplets (five of which have been calculated in the present work) originate from the latter dissociation channel. As could be expected from the electron distribution along the σ-frame, the $^5\Sigma^-(3)$ state coming from the Zn(^{1}S) + C(^{5}S) atomic fragments is repulsive, with a very shallow van der Waals minimum at 3.94 Å (Table 2). Close to 4 bohr, the $^5\Sigma^-(3)$ curve interacts strongly with a higher state of the same symmetry, but of unknown origin (Figure 1).

The $^3\Delta(2)$ state is the lowest state, T_e = 97.8 (101.3) kcal/mol at the MRCI [MRCI(d^{10})+Q level], from the Zn(^{3}P) + C(^{1}D) channel, sharing the same CFs of A_1 symmetry with the $^3\Sigma^+(2)$ state coming from the same channel. As a result, the charge distribution (Table 3), binding energies, and spectroscopic parameters (Table 2) are practically identical. The bonding is consistent with that shown in eq 11.

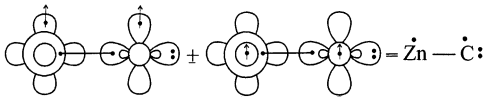

$$= \dot{Z}n - \dot{C}: \qquad (11)$$

$Zn(^3P; M_L=\pm1) + C(^3P; M_L=\pm1)$ $^3\Sigma^+(2)$ or $^3\Delta(2)$

The single σ-bond results in a binding energy of ~35−40 kcal/mol. We notice the ~0.2 e^- Zn-to-C transfer via the π-skeleton, with the return of ~0.1 e^- to Zn via the σ-skeleton. The next $^3\Delta$ state, $^3\Delta(3)$, is repulsive, stemming from the (0,±2) components and showing a van der Waals interaction of about 0.5 kcal/mol near 4 Å (Table 2).

Finally, we turn our attention to the remaining $^3\Pi(4)$ and $^3\Pi(5)$ PECs. A clear view of their morphology is shown in Figure 2. At infinity, these two states start with the (±1,0) and (0,±1) M_L components, respectively. Near 4.5 bohr, we observe a complicated avoided crossing among three states, $^3\Pi(4)$,

$^3\Pi(5)$, and the (noncalculated) $^3\Pi(6)$ curve. The $^3\Pi(4)$ state suffers two more avoided crossings, one already mentioned close to its equilibrium distance with the repulsive part of the $^3\Pi(3)$ state and another one at ~3 bohr, again with the $^3\Pi(5)$ state (at their repulsive parts) (Figure 2). As evidenced from the wave function compositions in Table 3, it is difficult to draw vbL icons for these two states due to their highly multireference character. The latter arises from the strong interactions among the $^3\Pi$ states that are energetically close to each other near the PEC minima. From Figure 2 and Table 2 we observe the existence of two minima of similar magnitude (~7 kcal/mol) for the $^3\Pi(5)$ state, a result of the strong avoided crossings this state suffers.

4. Conclusions and Remarks

In the present work we have studied the ground state and 29 excited states of the experimentally unknown ZnC molecule, employing multireference variational methods coupled with large basis sets (Roos-ANO-TZ/aug-cc-pVQZ). Full potential energy curves were calculated for all states with the purpose of obtaining binding characteristics and trends. Our main findings are summarized as follows:

(a) The ground state of ZnC is of $^3\Sigma^-$ symmetry with a binding energy D_e = 23.7 kcal/mol and a bond length r_e = 1.960 Å at the MRCI(d^{10})+Q level of theory, including one-electron Douglas−Kroll relativistic corrections. These results are in relative conformity with the QCISD(T) results of Boldyrev and Simons.[15] Due to near-degeneracy effects, the X $^3\Sigma^-$ state shows some multireference character, which cannot be ignored if one is after quantitative results. Zn and C are held together by a dative Zn-to-C σ bond.

(b) Contrary to the known controversies on the alkaline-earth metal carbide diatomics over the $^3\Sigma^-$ or $^5\Sigma^-$ identity of their ground states, no such controversy exists in ZnC; the $^5\Sigma^-$ state (originating from an excited ^{3}P Zn atom) is predicted to lie 26.3 or 23.8 kcal/mol, with or without relativistic effects [MRCI-(d^{10})+Q], above the ground X $^3\Sigma^-$ state. The reason for this larger $^5\Sigma^- \leftarrow$ X $^3\Sigma^-$ separation comes from the significant $^3P(4s^14p^1) \leftarrow {}^1S(4s^2)$ atomic energy gap of Zn, which is more than twice as large as that, for instance, in Ca. However, by upshifting the $^5\Sigma^-$ PEC by 5.2 (or 2.4 including relativistic effects) kcal/mol (Table 1) as to bring into coincidence the calculated and the experimental asymptotes, the $^5\Sigma^- \leftarrow$ X $^3\Sigma^-$ energy separation becomes as large as 29 kcal/mol, with the $^5\Sigma^-(1)$ state *not being the first excited-state anymore* (see Figure 4).

(c) Most of the low-energy ZnC spectrum is spanned by states tracing their origin to the Zn(^{3}P) + C(^{3}P) asymptotic limit. In the states where Zn participates with the excited $^3P(4s^14p^1)$ state, bonding is much more facilitated due to the availability of the 4p orbitals; thus, much deeper potential energy wells are observed, the larger one being 89.3 (90.4 including relativistic effects) kcal/mol ($^5\Sigma^-(1)$).

(d) A variety of bonding mechanisms is revealed ranging from a half to two bonds between Zn and C. The state with the shortest bond length (1.810 Å) is the $^3\Pi(2)$ state, having a formal bond order of 2 (1/2 σ-bond and 3/2 π-bonds). In almost all states coming from the $^3P(4s^14p^1)$ state of Zn, the 4s electron remains practically localized on Zn; usually, the same happens with C and its p_π electrons. The bonding between Zn and C is often the result of the strong $4p_z-2p_z$ electron interaction between the two atoms along the σ-frame. Zn is, in almost all states, the positive end of the molecule, acquiring in some cases positive charge up to +0.6.

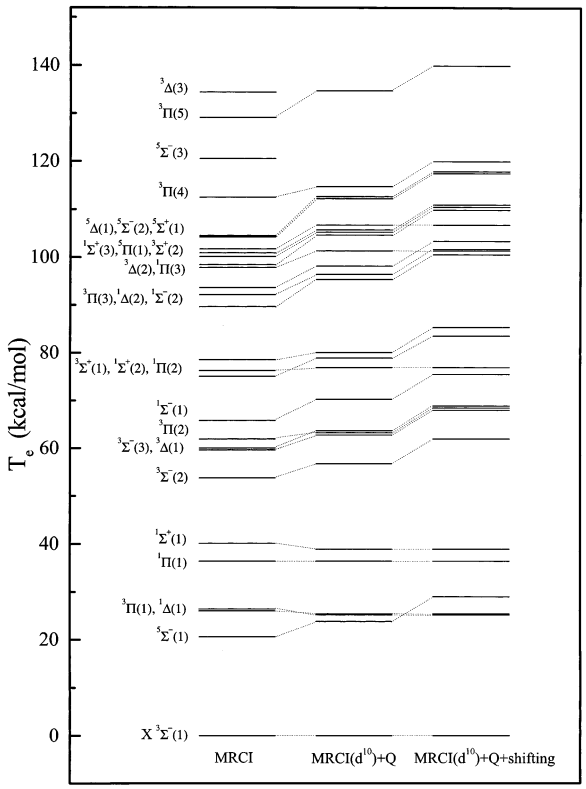

Figure 4. Relative energy levels of ZnC at the MRCI, MRCI(d^{10})+Q, and MRCI(d^{10})+Q+"shifting" levels of the Zn-asymptotes to match the experimental atomic separations.

(e) Correlating the $3d^{10}$ electrons of Zn results in shortening the Zn−C bond lengths by an impressive 0.06−0.09 Å, but the effect on the binding energies and energy separations seems rather unclear at first glance (Table 2). Careful examination, though, reveals that, whenever the in situ Zn is in the excited ^{3}P state, the $3d^{10}$ correlation increases D_e's and T_e's by 3−6 kcal/mol, while when Zn is in its ground ^{1}S state, these parameters remain practically unchanged, or even *decrease* by ~1−2 kcal/mol. We believe that the actual effect of the $3d^{10}$ electrons on the ZnC binding energies is probably about ±1 kcal/mol. The rest serves to "fix" the rather underestimated $^3P \leftarrow {}^1S$ atomic energy gap of Zn, as evinced from Table 1: indeed, the $3d^{10}$ electrons increase this gap toward the experimental value by ~0.4 eV or ~9 kcal/mol. Therefore, the $3d^{10}$ electrons apparently affect more dramatically the asymptotic limits rather than the PEC's equilibria. We could have "guessed" very similar T_e values if we were to shift our valence-only MRCI values to match the experimental $^3P \leftarrow {}^1S$ Zn gap. Now, by doing so to the MRCI(d^{10})+Q T_e values to correct for remaining correlation and relativistic effects, we reach our final shifted T_e values. The spectrum of ZnC as revealed by the classification of all bound states according to increasing energy is shown in Figure 4. Notice some differences in state orderings when moving from the MRCI, to MRCI(d^{10})+Q, to shifted MRCI(d^{10})+Q values. We believe that the latter should give a rather reliable state ordering and may facilitate the experimental detection of ZnC in the laboratory or the interstellar space; the X $^3\Sigma^-$ rotational constant B_e is 13.02 GHz at the MRCI(d^{10})+Q/Rel level. Possible observable Franck−Condon transitions could be the spin allowed $^3\Pi(2) \leftarrow$ X $^3\Sigma^-$ transition near 22 100 cm^{-1}, and the Ω allowed $^1\Delta(1) \leftarrow$ X $^3\Sigma^-$ transition near 8800 cm^{-1}.

Acknowledgment. I.S.K.K. expresses his gratitude to the Association of Greeks from Egypt (Σ.A.E.) for financial support.

References and Notes

(1) Kalemos, A.; Mavridis, A.; Harrison, J. F. *J. Phys. Chem. A* **2001**, *105*, 755.
(2) Kalemos, A.; Mavridis, A. *J. Phys. Chem. A* **2002**, *106*, 3905.
(3) Tzeli, D.; Mavridis, A. *J. Chem. Phys.* **2002**, *116*, 4901.
(4) Kerkines, I. S. K.; Mavridis, A. *J. Phys. Chem. A* **2000**, *104*, 11777.
(5) Kerkines, I. S. K.; Mavridis, A. *Collect. Czech. Chem. Commun.* **2003**, *68*, 387.
(6) Kerkines, I. S. K.; Mavridis, A. Manuscript in preparation.
(7) Papakondylis, A.; Mavridis, A. *J. Phys. Chem. A*, accepted.
(8) Kerkines, I. S. K.; Pittner, J.; Čarsky, P.; Mavridis, A.; Hubač, I. *J. Chem. Phys.* **2002**, *117*, 9733.
(9) Halfen, D. T.; Apponi, A. J.; Ziurys, L. M. *Astrophys. J.* **2002**, *577*, L67.
(10) Bauschlicher, C. W., Jr.; Langhoff, S. R.; Partridge, H. *Chem. Phys. Lett.* **1993**, *216*, 341.
(11) Borin, A. C.; Ornellas, F. R. *J. Chem. Phys.* **1993**, *98*, 8761.
(12) (a) Castro, M. A.; Canuto, S.; Müller-Plathe, F. *Phys. Rev. A* **1992**, *46*, 4415. (b) da Silva, C. O.; Teixeira, F. E. C.; Azevedo, J. A. T.; da Silva, E. C.; Nascimento, M. A. C. *Int. J. Quantum Chem.* **1996**, *60*, 433. (c) Serrano, A.; Canuto, S. *Chem. Phys. Lett.* **1997**, *269*, 193.
(13) Takada, H. H.; Pelegrini, M.; Roberto-Neto, O.; Machado, F. B. C. *Chem. Phys. Lett.* **2002**, *363*, 283.
(14) Moore, C. E. *Atomic Energy Levels*; NSRDS-NBS Circular No. 35; U.S. GPO: Washington, DC, 1971.
(15) Boldyrev, A. I.; Simons, J. *Mol. Phys.* **1997**, *92*, 365.
(16) Pou-Amerigo, R.; Merchan, M.; Nebot-Gil, I.; Widmark, P. O.; Roos, B. *Theor. Chim. Acta* **1995**, *92*, 149.
(17) (a) Dunning, T. H., Jr. *J. Chem. Phys.* **1989**, *90*, 1007. (b) Kendall, R. A.; Dunning, T. H., Jr.; Harrison, R. J. *J. Chem. Phys.* **1992**, *96*, 6796.
(18) Boys, S. F.; Bernardi, F. *Mol. Phys.* **1970**, *19*, 553.
(19) (a) Werner, H.-J.; Knowles, P. J. *J. Chem. Phys.* **1988**, *89*, 5803. (b) Knowles, P. J.; Werner, H.-J.; Reinsch, E. A. *J. Chem. Phys.* **1982**, *76*, 3144. (c) Werner, H.-J. *Adv. Chem. Phys.* **1987**, *LXIX*, 1.
(20) (a) Docken, K.; Hinze, J. *J. Chem. Phys.* **1972**, *57*, 4928. (b) Werner, H.-J.; Meyer, W. *J. Chem. Phys.* **1981**, *74*, 5794.
(21) Gdanitz, R. J.; Ahlrichs, R. *Chem. Phys. Lett.* **1988**, *143*, 413.
(22) (a) Douglas, M.; Kroll, N. M. *Ann. Phys. (N. Y.)* **1974**, *82*, 89. (b) Hess, B. A. *Phys. Rev. A* **1985**, *32*, 756. (c) Hess, B. A. *Phys. Rev. A* **1986**, *33*, 3742.
(23) de Jong, W. A.; Harrison, R. J.; Dixon, D. A. *J. Chem. Phys.* **2001**, *114*, 48.
(24) ROVIB is a program for solving the rovibrational Schrödinger equation written by A. Papakondylis and developed in the present laboratory.
(25) Amos, R. D.; Bernhardsson, A.; Berning, A.; Celani, P.; Cooper, D. L.; Deegan, M. J. O.; Dobbyn, A. J.; Eckert, F.; Hampel, C.; Hetzer, G.; Knowles, P. J.; Korona, T.; Lindh, R.; Lloyd, A. W.; McNicolas, S. J.; Manby, F. R.; Meyer, W.; Mura, M. E.; Nicklass, A.; Palmieri, P.; Pitzer, R.; Rauhut, G.; Schütz, M.; Schumann, U.; Stoll, H.; Stone, A. J.; Tarroni, R.; Thorsteinsson, T.; Werner, H.-J. MOLPRO—a package of ab initio programs designed by H.-J. Werner and P. J. Knowles, version 2002.3.
(26) Bunge, C. F.; Barrientos, J. A.; Bunge, A. V.; Cogordan, J. A. *Phys. Rev. A* **1992**, *46*, 3691.
(27) Tzeli, D.; Mavridis, A. *J. Chem. Phys.* **2003**, *118*, 4984.